

Aluminum-based hot carrier plasmonics

Tao Gong^{1,2} and Jeremy N. Munday^{1,2,a)}

¹*Department of Electrical and Computer Engineering, University of Maryland, College Park, Maryland 20742, USA*

²*Institute for Research in Electronics and Applied Physics, University of Maryland, College Park, Maryland 20742, USA*

(Received 23 October 2016; accepted 27 December 2016; published online 13 January 2017; corrected 20 January 2017)

Aluminum has recently arisen as an excellent alternative plasmonic material due to its tunability, low optical loss, and CMOS compatibility. However, its use in optoelectronic applications has been limited due to Al oxidation. Herein, we report a semiconductor-free aluminum hot carrier device that exploits the self-terminating oxidation to create an interface barrier for high performance metal-insulator-transparent conducting oxide devices. We find a 300% enhancement of the responsivity compared to similarly reported Au-based devices, resulting in a responsivity up to ~ 240 nA/W, and a clear dependence of the open-circuit voltage on incident photon energy. We show that further improvement can be obtained by coupling to plasmonic modes of a metal-insulator-metal structure composed of a nanowire array adjacent to a thin aluminum film, increasing light absorption by a factor of three and enabling tunability of the hot carrier response for improved device performance. Published by AIP Publishing. [<http://dx.doi.org/10.1063/1.4973814>]

Hot carrier-based devices, which take advantage of the excess kinetic energy of carriers (electrons or holes) excited directly from incident photons or by plasmon decay, have been drawing increasing interest over the recent years. They have extensive applications in photodetection,^{1–5} photovoltaics,^{6–11} photochemistry,^{12–17} hot carrier-induced phase transitions,¹⁸ and luminescence.¹⁹ Most of the devices consist of a metal-semiconductor Schottky junction or a metal-insulator-metal (MIM) junction. Hot carriers are generated in the metal upon excitation and are subsequently injected into the counter-electrode to form the photo-generated current. A nanostructured metal layer is usually employed to couple the incident light into localized surface plasmonic resonances (LSPRs) or surface plasmon polaritons (SPPs), i.e., oscillations of free electrons near the metal surface. The surface plasmon effect substantially enhances the field intensity and results in significantly enhanced light absorption and hot carrier excitation inside the metal.

From a materials' perspective, noble metals such as gold and silver are broadly utilized in plasmonic and hot carrier-based devices due to the efficient surface plasmon coupling at long wavelengths and their stability in air. However, recently aluminum-based plasmonics has become more attractive because of aluminum's broadband tunable plasmon response through the entire UV-VIS-NIR spectrum, especially in the UV range because of its low loss.^{20,21} Moreover, aluminum is a low-cost, naturally abundant material that can be fabricated on a large-scale with the mature fabrication technology of microelectronics.²² Yet, despite the increasing attention to aluminum plasmonics, few papers have explored aluminum-based hot-electron devices as photodetectors. Part of the reason is that aluminum oxidizes quickly upon exposure to air,^{20,23} which prohibits the hot electron extraction from inside the aluminum layer.

Here, we present a simple device structure in which an Al thin film is employed for generating hot electrons upon photon excitation. The excited hot electrons are subsequently injected into a counter-electrode made of a transparent conducting oxide (TCO), in our case indium tin oxide (ITO). The two electrodes are separated by an ultra-thin layer of alumina formed by direct native oxidation of the surface of the Al film and subsequent oxygen plasma treatment. The device shows a peaked photoresponse at short wavelengths near the UV region, indicating its potential application in short-wavelength photodetection. A shift of the open-circuit voltage (V_{OC}) with respect to the incident photon energy and linearly increased photocurrent with increasing incident power are observed to further confirm the hot electron effect. In addition to these experimental results, we propose a design that can further improve the performance by placing nanowire arrays on top of the Al-insulator-ITO structure, which couples the incident light into plasmon modes in the Al film. This design significantly increases the light absorption in the near-IR wavelength regime. The combination of Al plasmonics and hot carrier effects will be advantageous for applications in photodetection, energy harvesting, etc.

Devices are made via thermal evaporation of a 30 nm Al film on a glass slide through a shadow mask with aligned strips to form the bottom electrodes. The samples are then exposed to air to form a 2–4 nm native oxide layer (i.e., alumina), followed by the oxygen plasma treatment under 100 W power and 5 Torr pressure in an oxygen plasma chamber. The ITO counter electrodes are sputtered onto the alumina film forming cross-junctions with the Al strips. Finally, a thin metallic wire is attached to the Al electrode with Epoxy CW2400 glue immediately after the deposition, and an ohmic contact is confirmed by resistivity measurements.

Optical absorption is measured in a 6 in. Labsphere integrating sphere with a Thermo Oriel Xenon lamp as the light source. For photocurrent measurements, the light source is a Fianium WhiteLase Supercontinuum laser. A SR830 Digital

^{a)}Author to whom correspondence should be addressed. Electronic mail: jnmunday@umd.edu

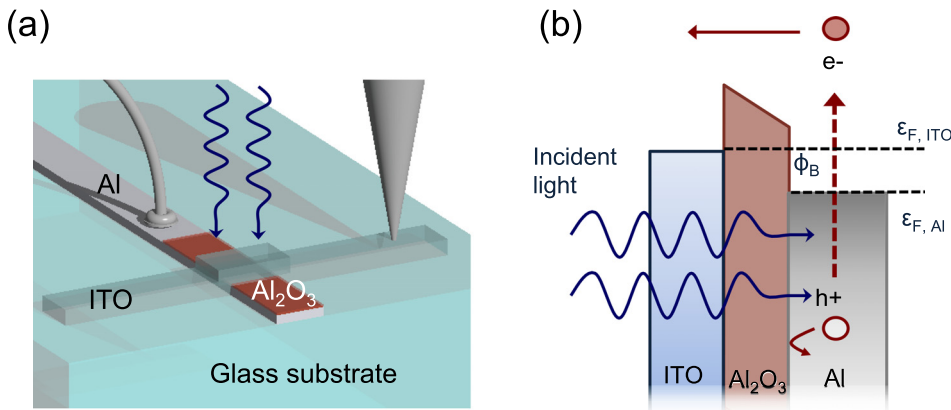


FIG. 1. (a) Schematic of the Al-Al₂O₃-ITO junction. Light illuminates the junction through the transparent ITO layer, exciting hot electrons at the Al-Al₂O₃ interface. (b) Schematic of the hot electron generation and transport through the oxide barrier.

lock-in amplifier, in conjunction with a Keithley 2400 Source Meter, is used for probing the photo-generated current with a bias voltage across the junction.

The schematic of the device junction is shown in Fig. 1(a). The incident light illuminates the Al-Al₂O₃ interface after passing through the ITO film, because ITO is nearly transparent throughout the visible spectrum. An exponential decay of the electric field at the Al surface leads to strong absorption at the interface and excitation of hot electrons. Note that this exponential decay arises from the penetration of the electric field within the skin depth, and not due to the surface plasmon excitation, because there are no momentum-compensation structures to couple the incident photons into plasmons for this geometry. The exponential absorption profile is beneficial for the subsequent injection of the hot electrons across the oxide barrier, because most of the excited hot electrons are spatially distributed at the Al-Al₂O₃ interface and will not lose much energy during the ballistic transport within the carrier mean free path (generally within few tens of nanometers but also varies with carrier energy²⁴). The injected hot electrons will be collected by the counter electrode, i.e., ITO, forming the photocurrent (Fig. 1(b)). The barrier height seen by the hot holes is much larger than that of the hot electrons due to the large bandgap (6–8.3 eV) of Al₂O₃.²⁴ Therefore, the collected photocurrent is mostly attributed to the unidirectional hot electron flow from Al to ITO. A similar transparent conducting oxide-based structure using gold has been shown to outperform the pure metal-insulator-metal (MIM) counterpart for the above reasons.^{3,6}

Figure 2 shows the calculated and experimental absorption spectrum of the device. A finite-difference-time-domain (FDTD) simulation was performed to calculate the light absorption in each layer of the stack at normal incidence, as shown in Fig. 2(a). It is the absorption difference between the two electrodes that determines the hot electron injection efficiency. As shown in the inset of Fig. 2(a), the absorption difference does not vary much over the visible wavelength range. The total absorption also shows little variation under oblique illumination over a broad range of incident angles (Fig. 2(b)). This angular independence is a great advantage for both photodetectors and solar light harvesting, where there is a large portion of solar power coming from diffuse light due to the atmospheric scattering.

The generated photocurrent depends not only upon the absorption of light, but also upon the internal injection efficiency of the excited hot electrons. Upon excitation, the hot electrons will redistribute their energy based on their initial energy states in the metal. Recent studies of hot carrier generation in various materials and nanostructures have explored their hot carrier energy redistribution and carrier dynamics.^{25–29} As the hot electrons travel toward the Al-Al₂O₃ interface, electron-electron scattering further redistributes their energy and momentum,^{8,24} which can reduce their probability of reaching the interface. Upon reaching the interface, the probability of injection through the barrier is mainly dependent on the barrier height and the energy and momentum of the hot electrons.^{7,8} All of the above effects act together to determine the injection efficiency and the final photoresponse. As shown in Fig. 3(a), although the absorption difference does

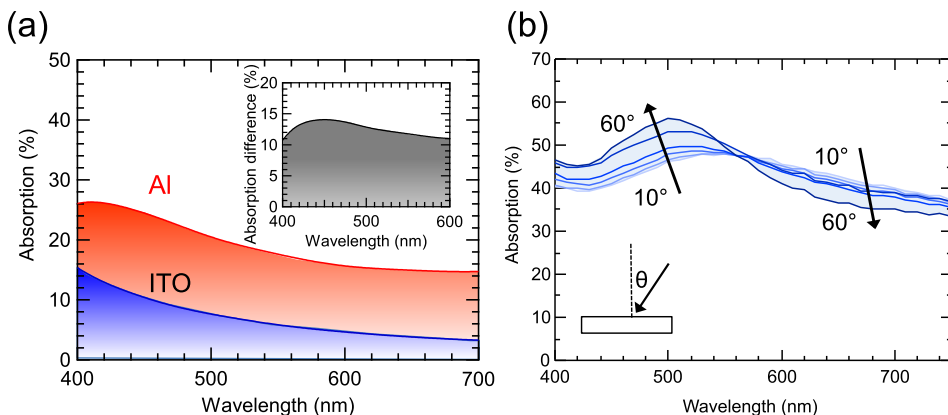


FIG. 2. Absorption spectrum of the device. (a) Calculated absorption in Al (red) and ITO (blue). Inset shows the absorption difference between Al and ITO does not vary much with the wavelength. (b) Experimental total absorption versus the wavelength for different incident illumination angles (10° to 60° in 10° steps). The absorption is nearly independent of the incident angle.

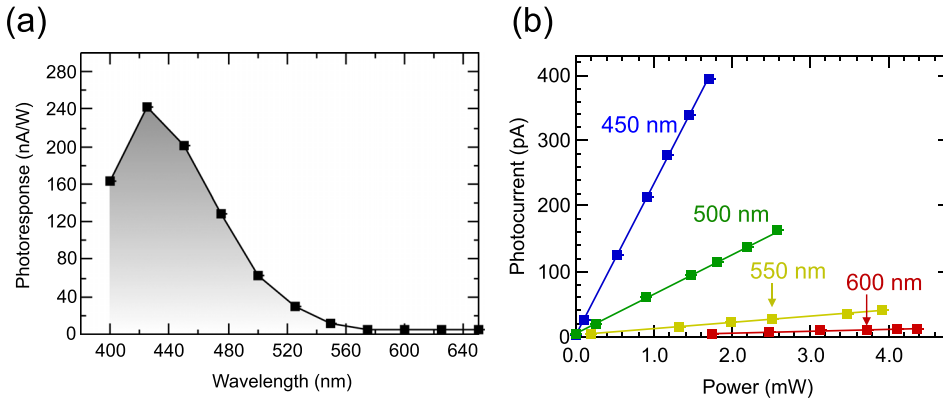


FIG. 3. (a) Photoreponse of the device under monochromatic illumination. The device shows much higher response at short wavelengths because more hot electrons are excited to high energy states, which lead to higher injection efficiency. (b) Photocurrent scales linearly with the incident light power.

not vary much with the illumination of different energy photons, the photoresponse peaks at short wavelength. This is because hot electrons are promoted to higher energy states when excited by higher energy photons, therefore a larger proportion of them are injected to form the photocurrent. The high sensitivity to short-wavelength incident illumination makes the device an excellent candidate for applications in photodetection. Hot electron generation and extraction is a linear process, i.e., one absorbed photon excites only one hot electron. This is confirmed by the linear relation between the photocurrent and the incident light power (Fig. 3(b)).

The photoresponse of the device also depends on the bias voltage across it as a result of the changing barrier height at the Al-Al₂O₃ interface under bias (Fig. 4(a)). An approximately linear decrease of photocurrent is observed with an increasing bias voltage. The linearity indicates a nearly uniform energy distribution of hot electrons above the Fermi energy in Al. This uniform energy distribution has also been demonstrated theoretically.^{26,27} Unlike many noble metals, such as Au and Ag, in which the hot carrier energy distribution has peaks due to d-band transitions, the d-band in Al lies above its Fermi level. This allows for the direct intraband transitions to states with energies ranging continuously from the Fermi level to one photon energy above the Fermi energy.^{4,25,30}

The open-circuit voltage V_{OC} , i.e., the voltage at which the total photocurrent reaches zero while the device is illuminated, increases with the incident photon energy (Fig. 4(b)). This agrees with the approximation⁶

$$V_{OC} \simeq \frac{E_{ph} - \Phi_B}{e} \left(1 - \frac{I_{SC}^{bm}}{I_{SC}^{top}} \right), \quad (1)$$

where E_{ph} is the photon energy, Φ_B is the barrier height, I_{SC}^{bm} is the short-circuit current from bottom to top (ITO to Al), and I_{SC}^{top} is the short-circuit current from top to bottom (Al to ITO). The barrier height is estimated to be 1.5–1.6 eV by this equation. The surface quality, which is affected by pinholes, traps, interlayer dipoles, etc., all influence the actual barrier height³¹ and is heavily dependent upon the oxide growth and treatment process. A photocurrent phase change of $\sim 180^\circ$ is observed in the measurement with a lock-in amplifier. This indicates the photocurrent transitions from positive to negative when the photocurrent from ITO exceeds that from Al (Fig. 4(a) inset).

To further enhance the light absorption, and hence the hot electron generation, we propose and simulate a device structure where a well-aligned nanowire array is placed on top of the planar Al-Al₂O₃-ITO device separated by a 20 nm insulating layer of Al₂O₃ (inset in Fig. 5(a)). This insulating layer prevents hot electrons from being directly extracted from the nanowires. Light is illuminated from above the nanowire arrays with electric field parallel to the wires (TM

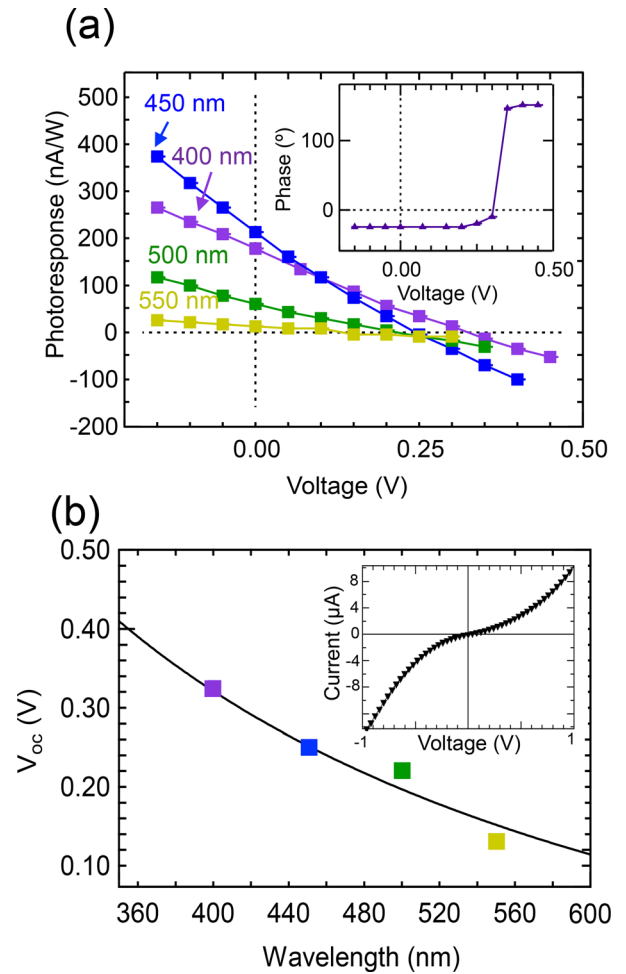


FIG. 4. (a) Photoreponse under monochromatic illumination with bias. The open-circuit voltage V_{OC} ranges from 0.10 to 0.35 V. Inset: The lock-in detector shows a 180° phase change of the measured photocurrent near V_{OC} . This behavior indicates that the photocurrent flow is reversed from ITO to Al under bias $>V_{OC}$. (b) V_{OC} varies with the incident illumination wavelength, with higher energy photons yielding a higher V_{OC} . Inset: dark current-voltage characteristic of device shows diode-like behavior.

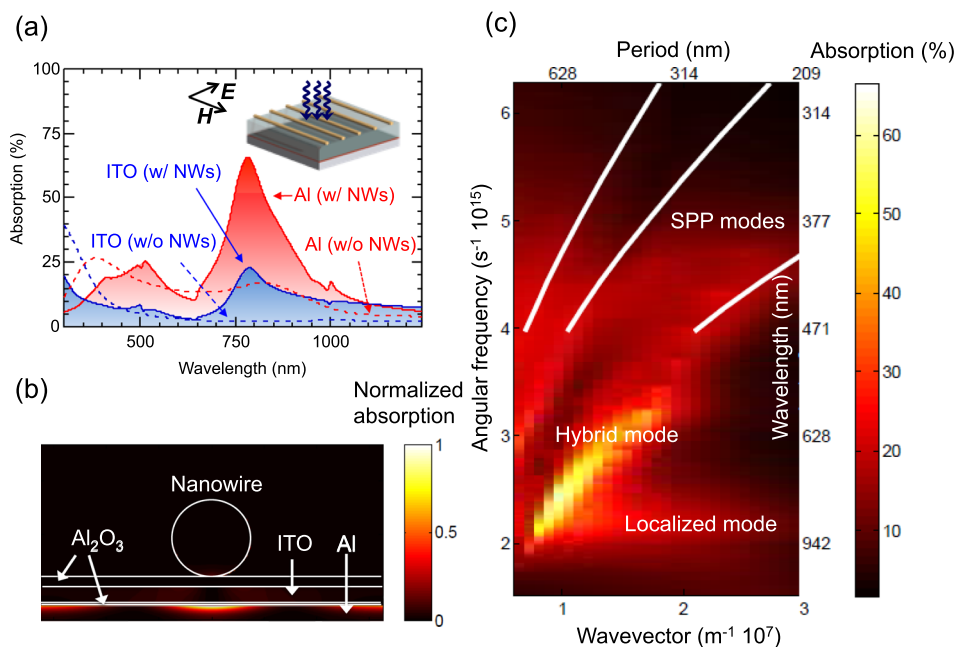


FIG. 5. (a) Absorption in the Al (red) and ITO (blue) films in the devices with Au nanowires (solid lines) and without nanowires (dashed lines). The absorption is enhanced at about 783 nm wavelength due to the coupling of incident light into plasmon modes. Inset shows the schematic of the device structure and the incident light polarization. (b) Absorption profile of the device (cross-section). The enhanced absorption is confined in the vicinity of the Al-oxide interface. (c) Absorption contour plot with varying wavelength and nanowire period. The SPP modes (white solid lines) are simulated with the FDTD mode solution. The most intensive absorption occurs where the SPP modes and the localized mode coincide and interact, which results in the hybrid mode.

polarization). With the nanowire array (diameter 150 nm and period 650 nm) on top, the absorption in Al is significantly enhanced in the near IR region with an absorption peak of 65.7% at a wavelength of 783 nm (Fig. 5(a)), approximately 4 times larger than that of the planar structure at the same wavelength (absorption of 16.2%) and nearly 3 times greater than the peak absorption of the planar device. The solar spectrum integrated absorption is also increased by $\sim 50\%$ with the addition of the nanowires. The enhanced absorption occurs in the Al at the Al-Al₂O₃ interface (Fig. 5(b)), which is beneficial for the traversal of the generated hot electrons before losing much energy. To study the cause of the enhancement, a dispersion-relation contour plot (Fig. 5(c)) is obtained by plotting the calculated absorption spectrum in the Al film while varying the period of the array. The three branches where the absorption enhancement scales with array period indicate that they are the Bragg-SPP modes, which depend on the diffraction condition imposed by the lattice parameter, i.e., the period of the array in our case.^{32,33} The FDTD mode simulation of the SPP modes (white solid lines) agrees well with the absorption enhancement. On the other hand, an absorption enhancement that is nearly independent of the nanowire array period occurs at a wavelength of ~ 850 nm. This period-independent absorption indicates a localized plasmon mode of the individual unit cell.³² However, the most intense absorption ($\sim 65.7\%$ at 783 nm) results from the strong interaction between the SPP modes and the localized mode when the two coincide, leading to the hybrid mode (Fig. 5(c)).³² This hybrid mode boosts the absorption significantly and therefore enhances the hot electron generation. Another advantage of this design is that the resonance intensity and wavelength can be tuned by modifying the coupling of these modes through further optimization of the period and diameter of the nanowires.

In conclusion, we fabricated an aluminum-based hot electron device and demonstrated efficient hot electron excitation and collection in a planar structure. An open-circuit voltage shift with incident photon energy is also observed.

These results are promising for applications of hot electron effects in aluminum for photodetection and photovoltaics. Furthermore, we showed that nanowires can be used to couple the incident light into plasmonic modes leading to strong absorption enhancements, enabling tunability of the resonance throughout the VIS-NIR.

The authors acknowledge funding support from the Office of Naval Research under Grant No. N00014-16-1-2540 and the National Science Foundation under Grant No. ECCS-1554503.

- ¹M. W. Knight, H. Sobhani, P. Nordlander, and N. J. Halas, *Science* **332**, 702–704 (2011).
- ²H. Chalabi, D. Schoen, and M. L. Brongersma, *Nano Lett.* **14**, 1374–1380 (2014).
- ³T. Gong and J. N. Munday, *Nano Lett.* **15**, 147–152 (2015).
- ⁴C. Clavero, *Nat. Photonics* **8**, 95–103 (2014).
- ⁵M. L. Brongersma, N. J. Halas, and P. Nordlander, *Nat. Nanotechnol.* **10**, 25–34 (2015).
- ⁶F. Wang and N. A. Melosh, *Nano Lett.* **11**, 5426–5430 (2011).
- ⁷A. J. Leenheer, P. Narang, N. S. Lewis, and H. A. Atwater, *J. Appl. Phys.* **115**, 134301 (2014).
- ⁸T. P. White and K. R. Catchpole, *Appl. Phys. Lett.* **101**, 073905 (2012).
- ⁹F. P. G. de Arquer, A. Mihi, D. Kufer, and G. Konstantatos, *ACS Nano* **7**, 3581–3588 (2013).
- ¹⁰F. P. G. de Arquer, A. Mihi, and G. Konstantatos, *Nanoscale* **7**, 2281–2288 (2015).
- ¹¹M. S. Onses, A. Ramírez-Hernández, S.-M. Hur, E. Sutanto, L. Williamson, A. G. Alleyne, P. F. Nealey, J. J. de Pablo, and J. A. Rogers, *ACS Nano* **8**, 6606–6613 (2014).
- ¹²C. D. Lindstrom and X.-Y. Zhu, *Chem. Rev.* **106**, 4281–4300 (2006).
- ¹³S. Mukherjee, F. Libisch, N. Large, O. Neumann, L. V. Brown, J. Cheng, J. B. Lassiter, E. A. Carter, P. Nordlander, and N. J. Halas, *Nano Lett.* **13**, 240–247 (2013).
- ¹⁴L. Zhou, C. Zhang, M. J. McClain, A. Manjavacas, C. M. Krauter, S. Tian, F. Berg, H. O. Everitt, E. A. Carter, P. Nordlander, and N. J. Halas, *Nano Lett.* **16**, 1478–1484 (2016).
- ¹⁵M. Le, J. U. Kim, K. J. Lee, S. Ahn, Y.-B. Shin, J. Shin, and C. B. Park, *ACS Nano* **9**, 6206–6213 (2015).
- ¹⁶M. Honda, Y. Kumamoto, A. Taguchi, Y. Saito, and S. Kawata, *Appl. Phys. Lett.* **104**, 061108 (2014).
- ¹⁷C. Ng, S. Dligatch, H. Amekura, T. J. Davis, and D. E. Gomez, *Adv. Opt. Mater.* **3**, 1582–1590 (2015).

- ¹⁸Y. Kang, S. Najmaei, Z. Liu, Y. Bao, Y. Wang, X. Zhu, N. J. Halas, P. Nordlander, P. M. Ajayan, J. Lou, and Z. Fang, *Adv. Mater.* **26**, 6467–6471 (2014).
- ¹⁹S. Saeed, E. M. L. D. de Jong, K. Dohnalova, and T. Gregorkiewicz, *Nat. Commun.* **5**, 4665 (2014).
- ²⁰M. W. Knight, N. S. King, L. Liu, H. O. Everitt, P. Nordlander, and N. J. Halas, *ACS Nano* **8**, 834–840 (2014).
- ²¹G. Maidecchi, G. Gonella, R. P. Zaccaria, R. Moroni, L. Anghinolfi, A. Giglia, S. Nannarone, L. Mattera, H.-L. Dai, M. Canepa, and F. Bisio, *ACS Nano* **7**, 5834–5841 (2013).
- ²²K. Diest, V. Liberman, D. M. Lennon, P. B. Welander, and M. Rothschild, *Opt. Express* **21**, 28638–28650 (2013).
- ²³I. Zoric, M. Zach, B. Kasemo, and C. Langhammer, *ACS Nano* **5**, 2535–2546 (2011).
- ²⁴D. A. Kovacs, J. Winter, S. Meyer, A. Wucher, and D. Dising, *Phys. Rev. B* **76**, 235408 (2007).
- ²⁵A. Manjavacas, J. G. Liu, V. KulKarni, and P. Nordlander, *ACS Nano* **8**, 7630–7638 (2014).
- ²⁶R. Sundararaman, P. Narang, A. S. Jermyn, W. A. Goddard III, and H. A. Atwater, *Nat. Commun.* **5**, 5788 (2014).
- ²⁷T. Gong and J. N. Munday, *Opt. Mater. Express* **5**, 2501–2512 (2015).
- ²⁸P. Narang, R. Sundararaman, and H. A. Atwater, *Nanophotonics* **5**, 96–111 (2016).
- ²⁹A. M. Brown, R. Sundararaman, P. Narang, W. A. Goddard, and H. A. Atwater, *ACS Nano* **10**, 957–966 (2016).
- ³⁰C. N. Berglund and W. E. Spicer, *Phys. Rev.* **136**, A1030–A1044 (1964).
- ³¹R. T. Tung, *Appl. Phys. Rev.* **1**, 011304 (2014).
- ³²F. P. G. de Arquer, A. Mihi, and G. Konstantatos, *ACS Photonics* **2**, 950–957 (2015).
- ³³J. N. Munday and H. A. Atwater, *Nano Lett.* **11**, 2195–2201 (2011).